HC1 GB00 105 M6

The Patent Office

INVESTOR IN PEOPLE

GB00/3736

The Patent Office
Concept House
Cardiff Road
Newport
South Wales
NP10 8QQ

12/4

WIPO PCT

10/089929

I, the undersigned, being an officer duly authorised in accordance with Section 74(1) and (4) of the Deregulation & Contracting Out Act 1994, to sign and issue certificates on behalf of the Comptroller-General, hereby certify that annexed hereto is a true copy of the documents as originally filed in connection with the patent application identified therein.

In accordance with the Patents (Companies Re-registration) Rules 1982, if a company named in this certificate and any accompanying documents has re-registered under the Companies Act 1980 with the same name as that with which it was registered immediately before re-registration save for the substitution as, or inclusion as, the last part of the name of the words "public limited company" or their equivalents in Welsh, references to the name of the company in this certificate and any accompanying documents shall be treated as references to the name with which it is so re-registered.

In accordance with the rules, the words "public limited company" may be replaced by p.l.c., plc, P.L.C. or PLC.

Re-registration under the Companies Act does not constitute a new legal entity but merely subjects the company to certain additional company law rules.

Signed

Dated 1st November, 2000

PRIORITY DOCUMENT

SUBMITTED OR TRANSMITTED IN COMPLIANCE WITH RULE 17.1(a) OR (b)

Patents Form 1/77

Patents 7
(Rule 16)

RECEIVED BY HAND

The Patent Office

1/77

05OCT99 E481... F01/7700 0.00 9923428.8

The Patent Office
Cardiff Road
Newport
Gwent NP9 1RH

Request for grant of a patent

(See the notes on the back of this form. You can also get an explanatory leaflet from the Patent Office to help you fill in this form)

1.	Your reference	100441/WJN
2.	Patent application number *(The Patent Office will fill in this part)*	04 OCT 1999 **9923428.8**
3.	Full name, address and postcode of the or of each applicant *(underline all surnames)*	Thomas Swan & Company Limited Crookhall Consett. County Durham, DH8 7ND
	Patents ADP number *(if you know it)*	760242800l
	If the applicant is a corporate body, give the country/state of its incorporation	United Kingdom ~~4439758001~~
4.	Title of the invention	OPTICAL SWITCH
5.	Name of your agent *(if you have one)*	Page White & Farrer
	"Address for service" in the United Kingdom to which all correspondence should be sent *(including the postcode)*	54 Doughty Street London WC1N 2LS
	Patents ADP number *(if you know it)*	1255003
6.	If you are declaring priority from one or more earlier patent applications, give the country and the date of filing of the or of each of these earlier applications and *(if you know it)* the or each application number	Country / Priority application number *(if you know it)* / Date of filing *(day / month / year)* None
7.	If this application is divided or otherwise derived from an earlier UK application, give the number and the filing date of the earlier application	Number of earlier application / Priority application number *(if you know it)* / Date of filing *(day / month / year)*
8.	Is a statement of inventorship and of right to grant of a patent required in support of this request? *(Answer 'Yes' if:* *a) any applicant named in part 3 is not an inventor, or* *b) there is an inventor who is not named as an applicant, or* *c) any named applicant is a corporate body* *See note (d))*	YES

9.	Enter the number of sheets for any of the following items you are filing with this form. Do not count copies of the same document	
	Continuation sheets of this form	0
	Description	21
	Claim(s)	0
	Abstract	0
	Drawing(s)	11
10.	If you are also filing any of the following, state how many against each item.	
	Priority documents	0
	Translations of priority documents	0
	Statement of inventorship and right to grant of a patent (Patents Form 7/77)	0
	Request for preliminary examination and search (Patents Form 9/77)	0
	Request for substantive examination (Patents Form 10/77)	0
	Any other documents *(please specify)*	
11.	I/We request the grant of a patent on the basis of this application.	
	Signature Date 04.10.99	
	PAGE WHITE & FARRER	
12.	Name and daytime telephone number of person to contact in the United Kingdom	W J Neobard 0171-831-7929

Warning

After an application for a patent has been filed, the Comptroller of the Patent Office will consider whether publication or communication of the invention should be prohibited or restricted under Section 22 of the Patents Act 1977. You will be informed if it is necessary to prohibit or restrict your invention in this way. Furthermore, if you live in the United Kingdom, Section 23 of the Patents Act 1977 stops you from applying for a patent abroad without first getting written permission from the Patent Office unless an application has been filed at least 6 weeks beforehand in the United Kingdom for a patent for the same invention and either no direction prohibiting publication or communication has been given, or any such direction has been revoked.

Notes

a) *If you need help to fill in this form or you have any questions, please contact the Patent Office on 0645 500505.*

b) *Write your answers in capital letters using black ink or you may type them.*

c) *If there is not enough space for all the relevant details on any part of this form. please continue on a separate sheet of paper and write "see continuation sheet" in the relevant part(s). Any continuation sheet should be attached to this form.*

d) *If you have answered 'Yes' Patents Form 7/77 will need to be filed.*

e) *Once you have filled in the form you must remember to sign and date it.*

f) *For details of the fee and ways to pay please contact the Patent Office.*

Optical Switch

The development of optical fiber switching components is vital to the continued growth of our global information systems. Single-stage matrix switches operating independently of the optical bit-rate and modulation formats, capable of reconfigurably interconnecting N optical inputs to M optical outputs (where N and M are generally, but not necessarily the same number), are particularly attractive. Many of the methods for achieving the required switching are limited in functional size to less than 16x16, and/or suffer from relatively poor noise performance. One method which provides good noise performance and is potentially more scalable than other optical switch technologies is to use reconfigurable holograms as elements for deflecting optical beams in free-space between arrays of optical inputs and optical outputs. A holographic optical switch of this form is shown in figure 1.

In figure 1, an array of optical sources (1) and an array of optical receivers (7) are arranged as the inputs and outputs of a holographic switch. For many applications, the sources and receivers may comprise cleaved or end-polished fibres. In other applications, the inputs may be light emitting sources such as lasers or LEDs, and the outputs may be photo-detectors. Each input (1) may transmit a different digital or analog optical signal through the switch to one (or possibly several) of the outputs (7). Thus up to N different signals may be simultaneously passing through the switch at any instant. Each input may consist of a single-wavelength modulated by data; a number of different data sources operating at different wavelengths (eg. a wavelength-multiplexed system); or a continuum of wavelengths. Although the switch is shown in cross-section in figure 1, the input & output arrays (1)(7) are typically 2-dimensional arrays, and the holographic switch comprises a 3-dimensional volume.

To achieve switching, the input array (1) is arranged behind a lens array (2). Each optical signal emitted by the input array enters free-space, where it is collimated by one of the lenses in lens array (2). Each collimated beam then passes through a hologram device (3). The device (3) displays a holographic pattern of phase and/or intensity and/or birefringence which has been designed to produce a specific deflection of the optical propagation directions of the beams incident upon the device. The hologram pattern may also be designed such that each optical beam experiences a different angle of deflection. The device (3) may also have the effect of splitting an individual beam into several different angles or diffraction orders. One application for utilising this power splitting effect is to route an input port to more than one output port.

The deflected optical signals propagate in free-space across an interconnect region (4) until they reach a second hologram device (5). The hologram pattern at (5) is designed in such a way to reverse the deflections introduced at plane (3) so that the emerging signal beams are parallel with the system optic axis again.

The optical signals then pass through lens array (6) where each lens focuses its associated optical signal into the output ports of receiver array (7). Thus the hologram pattern displayed on device (3) and the associated "inverse" hologram pattern displayed on device (5) determine which output fibre or fibres (7) receive optical data from which input fibre or fibres (1). The interconnect region (4) allows the signal beams to spatially reorder in a manner determined by the specific hologram patterns displayed on devices (3)(5). The switch also operates reversibly such that outputs (7) may transmit optical signals back to the inputs (1).

The system shown in figure 1 (and functionally equivalent configurations utilising planes of symmetry within the switch optics) is well known as a method for static optical shuffle, whereby devices (3)(5) are fixed hologram recordings and whereby the input signals are "hard-wired" to specific outputs. An extension of this optical shuffle provides a reconfigurable switch by means of displaying hologram patterns on a spatial light modulator. There are, however, some practical design problems associated with the migration from a static optical shuffle to a reconfigurable switch. In particular:

1) In order to implement such a holographic switch an appropriate set of hologram patterns must be chosen. This hologram set must be capable of routing any input channel to any input channel whilst keeping the insertion loss and crosstalk figures within specified values. This is not a straightforward task as the noise isolation between channels depends heavily on the patterns being used. In particular, the hologram set must be optimised to prevent higher order diffraction beams being launched down the wrong channel.

2) The maximum angular deflection that can be generated by a reconfigurable hologram is typically less than can be achieved by a fixed hologram recording. The length of interconnect region (4) between hologram planes (3)(5) is determined by this maximum angular deflection, and therefore a switch typically requires a greater free-space optical path-length than an optical shuffle. Because of component tolerances and packaging design constraints, it is often highly desirable to minimise this optical path-length.

3) The diffraction efficiency of a reconfigurable hologram is typically less than 100%, with some proportion of the shortfall exhibited as an undeflected "zero-order" signal passing straight through hologram devices (3)&(5). Without further enhancement to the switch, these undeflected signals give rise to unwanted noise signals in the receivers, eg. a fraction of the signal from input 1 always reaches output 1 irrespective of the hologram states, a fraction of the signal from input 2 always reaches output 2, etc. These signals corrupt the proper functioning of the switch.

4) A convenient method of constructing reconfigurable holograms for use within an NxN switch is to integrate a layer of liquid crystal material above a silicon circuit. This type of SLM typically operates in reflection rather than transmission, and the switch layout shown in figure 1 is therefore no longer appropriate.

5) The technique of polarization insensitive binary phase modulation using a ferroelectric liquid crystal is known.. The maximum theoretical diffraction efficiency for such a device is only 40.5%. However, in order to minimise the insertion loss of the switch and reduce crosstalk restrictions it is desirable to that continuous phase patterns can be displayed on the SLM.

In one aspect of the invention, the limitations outlined in 1-5 above are eased or eliminated by the adoption of a new scalable switch configuration based on two holographic beam steering devices in which the hologram patterns are chosen using a novel design algorithm. Phase only holograms are defined by a pixellated base-cell pattern. The base cell is directly calculated from the coordinates of the main replay spot for the desired hologram and is constructed using a rapid phase-quantisation procedure. The switch may be implemented using either micro-optics (as illustrated in figure 1) or bulk optical elements. In addition, the spatial light modulator may be binary, multiple or continuous phase.

We address some of the practical design problems associated with implementing such a holographic optical routing switch. A bulk optics implementation is included as a design example, and equations are disclosed which specify the optical design requirements of the invention. Further enhancements are then disclosed in order to reduce the physical length of the free-space interconnect region and ease switch packaging issues. These enhancements involve the introduction of one additional lens, which may also be conveniently offset to solve the crosstalk issue created by the hologram zero-orders. A layout applicable to the use of reflective holograms constructed using a layer of ferroelectric liquid-crystal or nematic liquid-crystal integrated above a semiconductor modulator array is disclosed.

We also describe in detail the operation of a novel reflective continuous phase nematic liquid crystal device designed to be used with such a holographic routing switch. The pixelated spatial light modulator is polarisation insensitive, addressing the limitation described in point 5 above. Finally, the procedure required to design the hologram set for a N×N holographic switch is outlined.

The basic configuration of an NxN holographic switch is shown in figure 2. The holograms have been omitted from this schematic for clarity. In figure 2, an array of optical sources (1) form the inputs of the switch and an array of optical sinks or receivers (9) form the outputs in a similar way to shown in figure 1. In the case of fibre-to-fibre switching: arrays (1)(9) may contain fibres that have been cleaved or end-polished at an angle to reduce back reflections; may be anti-

reflection coated; or may consist of a waveguiding device to adapt the optical signals to the correct positions and spacings. Alternatively, some construction for producing 2-dimensional fibre arrays may be used.

Following input (1), the array of optical signals enter free-space where they are collimated by a lens (2) which has a focal length of f_2. Input array (1) is typically arranged in the back focal plane of lens (2) at a distance f_2 from the principal surface of the lens such that the signal beams are collimated in different angular directions. Following lens (2), the collimated signals propagate in free-space fan-out region (3) towards lens (4). The signals propagating in region (3) are angularly dispersed by lens (2) in such a manner that the collimated beams are completely spatially separated by the time they reach (4). The location of lens (4) relative to lens (2) is chosen such that the beams pass across interconnect region (5) parallel to one another. Typically this condition is met by locating the principal surface of lens (4) a distance f_2+f_4 away from the principal surface of lens (2), where f_4 is the focal length of (4). An array of focused spots is then typically formed in the front focal plane of lens (4), somewhere within region (5).

Following interconnect region (5), lens (6) recollimates the signals and feeds them into fan-in region (7) where they are focused by lens (8) into the appropriate output fibres (9). Lens (8) is typically located a distance f_6+f_8 in front of lens (6), and outputs (9) are located in the focal plane of lens (8). In practice each of the lenses (2)(4)(6)&(8) may consist of a single bulk element or equivalent component with optical power such as cemented achromats, compound lens systems, and/or mirror elements. In addition, when the input sources (1) and output receivers (9) have the same optical numerical aperture of emission and light acceptance respectively (eg. the inputs and outputs are single-mode fibres) then lens (2) will have a similar specification as lens (8), and lens (4) will have a similiar specification as lens (6). In this case, a focal plane will exist exactly midway between lenses (4) and (6).

The switch is now constructed by arranging the reconfigurable hologram devices (10) and (11) about interconnect region (5) as shown in figure 3. Devices (10)&(11) should typically be located as close as possible to lenses (4)&(6) but may be placed on either side of these lenses respectively.

Devices (10) and (11) display various patterns of phase and/or intensity and/or birefringence which have been designed to deflect the optical propagation directions of the beams incident upon the devices. At any instant, the hologram pattern displayed at (11) must be designed to reverse the deflections introduced at device (10). Thus the deflections introduced by the holograms cause the input signals to be re-ordered and routed to the outputs in a manner according to the hologram patterns displayed. As the hologram patterns are changed, so is the routing of the switch. According to this embodiment of the invention, optical switching is achieved without the need for lens array components.

Design equations for constructing an NxN switch are now discussed for the situation where the optical signal beams have Gaussian TEM_{00} profiles. A Gaussian beam is the usual optical profile emitted by lasers and cleaved single-mode fibres. As a paraxial Gaussian propagates in free-space between lenses, its radial dimension changes but its profile remains Gaussian according to the following well-known propagation rule:

$$w = w_o \sqrt{1 + \left(\frac{\lambda z}{2\pi w_o^2} \right)^2} \qquad (1)$$

where w_o is the Gaussian waist dimension (minimum beam radius) arbitrarily located at z=0,
w is the transverse beam radius at location z/2,
z/2 is the propagation distance from the waist,
λ is the central optical wavelength of the optical signal beams.

For applications where the optical switch system described above (and shown in figures 2 and 3) is designed symmetrically, then each signal beam will form a Gaussian waist of diameter 2w exactly midway between hologram devices (10)&(11) at the centre of interconnect region (5), as shown in figure 4. For an interconnect distance z between holograms, the beams at planes (10)&(11) will have Gaussian diameters of 2w given by equation (1). In addition, if the distances between lens (4) and hologram (10), and between lens (6) and hologram (11) are negligible, then f_4 and f_6 should both be chosen to be equal to z/2.

Typically it is desirable make the inter-spacing, Δh, of the optical signals at planes (10)&(11) as small as possible to shorten the interconnect length. However, it is also desirable to increase this same dimension to reduce crosstalk between adjacent signals. Figure 5 is a plot of the expected noise isolation between any 2 adjacent optical paths given aberration-free optics. Parameter γ is defined as:

$$\gamma = \frac{\Delta h}{w} \tag{2}$$

A system design limit of $\gamma \geq 3$ is often acceptable, giving rise to about 39dB of noise isolation between adjacent signal paths or better. According to this invention, there is an optimum (minimum) value for Δh for a given value of γ found by equating the first deriative of equation (1) to zero:

$$\Delta h = \gamma \sqrt{\frac{\lambda z}{\pi}} \tag{3}$$

In addition, if the hologram devices are pixellated then there exists a maximum useful angle of diffraction, ϕ, that can be introduced by these devices. This angle ultimately determines the minimum interconnect length, z, that sustains correct operation of the switch:

$$\phi \approx \frac{\lambda}{2d} \qquad z \approx \frac{A}{\phi} \tag{4}$$

where d is the hologram pixellation pitch,
A is the total used hologram aperture.

In the general case, devices (10)(11) may introduce angular diffraction about just one, or both, axes of rotation and the hologram pixellation pitch may differ between the x and y axial directions.

Equations (2) through (4) lead to a design criteria in terms of the required interconnect length versus the number of inputs & outputs that can be supported. For the case where there are N inputs and N outputs arranged on regular 2-dimensional square-grids, the paraxial solution is:

$$z \approx \Delta h\left(\frac{2d\sqrt{N}}{\lambda}\right) \approx 4Nd^2\left(\frac{\gamma^2}{\pi\lambda}\right) \tag{5}$$

Thus a 32x32 switch constructed using holograms with 20µm feature size, operating at a central wavelength of 1.55µm, and with γ=3, requires the hologram devices (10)(11) to be spaced apart by at least 95mm. The insertion loss of the switch then increases gradually as the injected wavelength deviates from the design wavelength.

Equation (5) is the minimum optical path-length design for a holographic optical switch. A full design cycle for the switch must however also incorporate a procedure for determining an appropriate set of hologram patterns. This hologram set must typically be at least capable of routing any input to any output according to the capabilities of the hologram devices used, whilst also maintaining various switch performance targets such as the noise isolation between all optical paths and the insertion loss variability as the switch is reconfigured. Under these constraints, the hologram set may not utilise the full range of deflection angles that are available from the hologram devices. In addition, spatial arrangements of the input and output ports other than 1:1 aspect ratio square-packed grids may be better optimised for some applications. Hence it may not be possible to achieve the minimum optical path-length design. For these embodiments, equation (5) should be modified to:

$$z \approx C\left(\frac{d\Delta h}{\lambda}\right) \approx C^2\left(\frac{\gamma^2 d^2}{\pi\lambda}\right) \tag{6}$$

where C represents a scale parameter to account for the properties of the chosen hologram set. C must typically be determined by iterative design of the relative input and output port locations.

Each input port of the switch illuminates a unique sub-aperture region of device (10) and each output port collects light from a unique sub-aperture region of device (11). Each sub-aperture must then contain a minimum number of hologram pixels in order to achieve the correct switching functionality Equation (7) represents the *minimum* number of hologram pixels that must be present per sub-aperture per axis of diffraction.

$$\text{Minimum number of hologram pixels per port per axis of diffraction} = \frac{\Delta h}{d} = \frac{C\gamma^2}{\pi} \tag{7}$$

A sample of known data points for high-performance switch designs (≈40dB noise isolation, <1dB loss variability) based on square-packed input/output arrays and utilising binary-phase hologram devices such as ferroelectric-liquid-crystal spatial-light-modulators (FLC-SLMs), is tabulated below (Table 1):

Switch Functional Size	Spatial Arrangement of Input & Output Ports	C	Minimum Number of Pixels per Hologram Device
3 x 3	3 x 1	24	207 x 1
9 x 9	3 x 3	24	207 x 207
32 x 32	3 x 11	60	516 x 1891

Table 1 – Requirements for switch layout.

The maximum angular deflection that can be generated by a reconfigurable hologram is typically less than can be achieved by a fixed hologram recording and a switch typically therefore requires a relatively long free-space optical path-length between hologram devices. According to further embodiments of the invention, details of which are shown in figures 6 and 7, the physical distance between hologram devices (10)(11) is reduced by introducing additional optical elements to the switch. In these two schemes, the length of interconnect region (5) and thereby the optical path-length of the switch are reduced by incorporating a fifth lens into the system:-

In figure 6 a lens element (12) with negative optical power is placed as a field lens in the centre of interconnect region (5), and lenses (4)(6) are replaced by lenses (13)(14) respectively with shorter focal lengths. Each of these lenses may consist in practice of a single bulk element or equivalent compound component with optical power such that:

$$\left(f_{13} + f_{14}\right) < \left(f_4 + f_6\right) \tag{8}$$

where f_{13} is the focal length of lens (13),
f_{14} is the focal length of lens (14).

The addition of lens (12) must compensate for the shorter focal lengths of (13)&(14). For the common case when f_{13} equals f_{14}, operation of the switch will be maintained when element (12) satisfies:

$$f_{12} = \frac{f_{13}^2}{2f_4 - 2f_{13}} \tag{9}$$

where f_{12} is the focal length of lens (12),
f_4 is the focal length of the lens being replaced.

An alternative configuration is shown in figure 7, where a lens element (15) with positive optical power is placed as a unity-conjugate relay lens in the centre of interconnect region (5), and lenses (4)(6) are replaced by lenses (16)(17) respectively with shorter focal lengths. Each of these lenses may consist in practice of a single bulk element or equivalent compound component with optical power such that:

$$\left(4f_{15} + f_{16} + f_{17}\right) < \left(f_4 + f_6\right) \tag{10}$$

where f_{15} is the focal length of lens (15),
f_{16} is the focal length of lens (16),
f_{17} is the focal length of lens (17).

In this second configuration the spatial ordering of the output ports must be mirror-reversed about both the x and y axes in order to remain functionally identical to the original switch design. The addition of lens (15) must compensate for the shorter focal lengths of (16)&(17). For the common case when f_{16} equals f_{17}, operation of the switch will be maintained when element (15) satisfies:

$$f_{15} = \frac{f_{16}^2}{2f_4 - 2f_{16}} \tag{11}$$

Using the same 32x32 switch example as earlier, the optial path-length between hologram devices (10)(11) can now be reduced as follows. According to figure 6, if $f_{13} = f_{14}$ = 18mm then the central concave element should be designed with a focal length of 5.5mm, and the interconnect length would be reduced from 95mm to 36mm. Alternatively according to figure 7, if $f_{16} = f_{17}$ = 18mm then the central convex element should be designed with a focal length of 5.5mm, and the interconnect length would be reduced from 95mm to 58mm. Although slightly longer, the latter configuration has the advantage that optical aberrations are often easier to control in a positive relay element than in a negative field element.

The diffraction efficiency of a reconfigurable hologram is typically less than 100% due to imperfect optical modulation and/or due to spatial deadspace within the hologram pattern. Some proportion of the efficiency shortfall is often exhibited as an undeflected "zero-order" signal passing straight through both hologram devices (10)(11). Without further enhancement to the switch, these zero-order signals can lead to the generation of unwanted crosstalk signals in the output ports and therefore corruption of the proper switch function.

According to a further embodiment of the invention, the switch configuration is altered so that the zero-order signals pass safely out of the optical aperture of the system. This enhancement is most simply achieved by offsetting the input and output arrays (1)(9) to opposite sides of the system optic axis (18) whilst all other components remain symmetrically on-axis as shown in figure 8. Thus according to figure 8, the optic axis (18) of the system passes through the centre of all lens elements in the switch, but the input array (1) is offset completely to one side of this axis, and the output array (9) is completely offset to the opposite side. In addition, it is apparent that the optimum aspect ratio for the input and output arrays, given the same maximum diffraction angle capability of the hologram devices, is now 1:2 rather than a square array because of the system asymmetry. This change in aspect ratio will typically be reflected in slightly higher design values of parameter C (see equation 6).

With the embodiment of figure 8 however, the optical system is required to operate in an off-axis manner which may lead to the introduction of performance-limiting optical aberrations. A configuration which is functionally identical but which allows the optical system to operate in a near-paraxial manner is to adopt the configuration shown in figure 9. According to this embodiment of the invention, the input and output arrays and all lens components remain symmetrically on-axis except the central field or relay lens element (12) or (15) which is laterally offset by a small amount.

According to figure 9, the switch is designed such that if a point (19) located on the optic axis in the plane of the input array emits an optical signal then it may be interconnected to a point (20) located on the optic axis in the plane of the output array by deflecting an optical beam through an angle $+\psi$ at device (10) and through an angle $-\psi$ at device (11). Angle ψ is a parameter determined by the switch designer in order to avoid zero-order crosstalk problems. Points (19) and (20) are typically located in the geometric centres of the input and output array regions respectively. The required lateral offset, α, of the central lens element, as shown in figure 9, is then:

$$\alpha = \left(2f_{12} + f_{13}\right) \times \psi \tag{12}$$

if the central element is a negative lens as per figure 6, or:

$$\alpha = f_{16} \times \psi \tag{13}$$

if the central element is a positive lens as per figure 7. In both cases ψ is measured in radians about the axis orthogonal to the direction of displacement of the central lens.

Devices such as multiple-quantum-well modulator arrays, accousto-optic and electro-optic cells and liquid-crystal modulators are all potentially suitable devices for displaying reconfigurable holograms. Hologram devices (10)&(11) may in actuality be a single hologram display, two individual hologram displays, or a multiplicity of displays. Ferroelectric liquid-crystal (FLC) displays are particularly well suited to holographic switches because they may be configured as phase holograms in a polarisation insensitive way. Polarisation insensitivity is particularly important for fibre-to-fibre switches where it is relatively difficult to control the polarisation states entering the switch. A thin layer of an FLC material may also be conveniently integrated above a semiconducting device as a spatial light

modulator (SLM). In this case, circuitry on the silicon chip acts as both addressable electrodes for modulating the liquid-crystal, and as mirrors for reflecting the incident light. Holographic switches constructed with FLC-SLMs can be reconfigured relatively quickly, but are intrinsically limited to binary phase states and may therefore exhibit high insertion losses.

Polarisation modulation of light using nematic liquid-crystals (NLCs) has also been reported for non-switching applications. These systems use either a pair of pixel-by-pixel aligned NLC-SLMs separated by a half-waveplate, or use a single NLC-SLM combined with a quarter-waveplate and a back reflecting mirror. Such devices are capable of producing near continuously-variable phase modulation between 0 and some upper limit. In the following section, two configurations for producing a holographic NLC-SLM are presented. These designs are ideally suited for holographic switching devices.

Polarisation insensitive phase modulation of light using nematic liquid crystals for adaptive optics applications has been reported for modulation operation in transmission and reflection using either one or two layers of liquid crystal respectively. Here we consider how this might be applied to optical switches using holographic phase gratings operating in the telecommunications long wavelength window at 1.5 μm. The basic principles are being discussed and possible configurations are presented.

a. Analogue Phase Modulation

We consider the propagation of a planar wavefront, travelling along the z-direction through a layer of nematic liquid crystal of uniform alignment (figure 10). The optical axis of the uniaxial nematic medium has been taken in the general case to tilt away from the x-direction (however on to the plane xOz). The tilt angle θ is electrically controllable by the voltage applied across the cell and it ranges in the interval $[0, \pi/2]$.

The two propagation modes travel along the z-direction with different velocities, which are determined by the indicatrix (index ellipsoid) construction as can be seen in the figure 10. The component of the field that is parallel to the y-axis experiences refractive index n_o whatever the tilt angle θ is, and therefore the phase delay caused to it by the cell is independent of the voltage across it (ordinary wave). On the contrary, the x-component of the field (extraordinary wave) experiences different refractive index n for different values of the tilt angle. In the figure 10, the refractive index n is given by the long axis of the indicatrix ellipse and therefore the following equation exists:

$$\frac{1}{n^2(\theta)} = \frac{\cos^2(\theta)}{n_o^2} + \frac{\sin^2(\theta)}{n_e^2} \tag{14}$$

Since $0 \le \theta \le \pi/2$, it follows that $n_o \le n(\theta) \le n_e$. The relative phase delay between the two components is then given by the equation:

$$\Delta\phi = k_0 d \Delta n \tag{15}$$

In equation (15), d is the thickness of the LC cell, k_0 the wavenumber of the field in the free space and $\Delta n = n(\theta) - n_0$. Since Δn is a function of the voltage across the cell, equation (15) shows that the applied voltage can continuously control the phase difference between the two components across the cell.

b. Polarisation Insensitive Phase Modulation

We can mathematically represent unpolarized light in terms of two arbitrary, incoherent, orthogonal, linearly polarised waves (i.e. waves for which the relative phase difference is not constant in time). We

would be able to modulate such light if we could apply the same phase delay to both these components. However, The configuration in figure 10, allows just one of the two components (x-component) to be properly phase-modulated since y-component always gains the same phase delay. A possible configuration that would allow for both components to be modulated then would be a double pass configuration as the one in figure 11 (for reflective mode of operation). In between the two passes a suitable rotator is introduced, which rotates both components through 90°. The combination of a quarter-wave plate (with an optical axis tilted out of the plane 0xz by 45°) and a mirror acts as a 90° rotator. Each of the two components travels through the cell with alternating orthogonal polarisation states in between the two passes. In this way both components gain totally the same amount of phase delay through the system since they both experience both refractive indices ($n(\theta)$ and n_o). In particular:

$$1^{st}\ component:\quad \Delta\phi_1 = \phi_{1,in} - \phi_{1,out} = \Delta\phi_{1st-pass} + \Delta\phi_{2nd-pass} = k_0 n(\theta) d + k_0 n_o d \tag{16}$$

$$2^{nd}\ component:\quad \Delta\phi_2 = \phi_{2,in} - \phi_{2,out} = \Delta\phi_{1st-pass} + \Delta\phi_{2nd-pass} = k_0 n_o d + k_0 n(\theta) d \tag{17}$$

In figure 11 the subsequent polarisation states of the x-component of the unpolarised light travelling through the double pass configuration is being shown. Note that the light exits the system being in the opposite orthogonal state. We can describe the above system using mathematical formulation in terms of Jones matrices. In order to do so, we write down the Jones matrix for each component of the system separately. It is easier to express all the matrices in one co-ordinate system assuming that the light travels only in one direction (positive z). A mathematically equivalent system would be the one shown in figure 12.

Note that two quarter-wave plates and two layers of liquid crystal have been introduced in the path of the light in order to describe mathematically the two passes of light through the system. Also, the matrix M that represents the mirror element has to accommodate, apart from the π phase change of the x- and y-components (normal incidence of e/m wave on a good conductor), the inversion of the y-axis as well. Therefore we can write for the M in the xyz system:

$$M = \begin{bmatrix} e^{j\pi} & 0 \\ 0 & e^{j\pi} \end{bmatrix} \cdot \begin{bmatrix} 1 & 0 \\ 0 & -1 \end{bmatrix} \tag{18}$$

The quarter-wave plates 1 and 2 in the systems x'y'z and x''y''z, respectively, can be written as (x' and x'' are the fast axes of the plates 1 and 2 respectively):

$$Q_1' = \begin{bmatrix} e^{j\frac{\pi}{2}} & 0 \\ 0 & 1 \end{bmatrix} \quad \text{(in the } x'y'z\text{)} \tag{19}$$

$$Q_2'' = \begin{bmatrix} e^{j\frac{\pi}{2}} & 0 \\ 0 & 1 \end{bmatrix} \quad \text{(in the } x''y''z\text{)} \tag{20}$$

We need to express these two arrays in the xyz system. This can be done using the rotational array R, which can be written as follows:

$$R = \begin{bmatrix} \cos\psi & \sin\psi \\ -\sin\psi & \cos\psi \end{bmatrix} \tag{21}$$

Where:

$$\psi = 45° \tag{22}$$

Then the quarter-wave plates can be expressed in the xyz system as:

$$Q_1 = R^T Q_1' R \tag{23}$$

$$Q_2 = R Q_2' R^T \tag{24}$$

With R^T we note the transverse array of R.

Finally, the expressions for the two NLC cells, in the xyz system, will be identical (due to the uniaxial symmetry of the liquid crystal) and will be given by the equation:

$$N_1 = N_2 = \begin{bmatrix} e^{j(k_o n d)} & 0 \\ 0 & e^{j(k_o n_o d)} \end{bmatrix} \tag{25}$$

Note that the combination of the quarter-wave plate and the mirror acts as a 90° rotator of the two orthogonal components of light. Indeed, if we take the representation matrices for these two components (including both passes) we have:

$$A = Q_2 M Q_1 = R Q_2'' R^T M R^T Q_1' R \tag{26}$$

By substitution of the equations (18)-(22) we get:

$$A = \begin{bmatrix} 0 & 1 \\ 1 & 0 \end{bmatrix} \tag{27}$$

which delivers the rotational functionality that we need, since:

$$\begin{bmatrix} 1 \\ 0 \end{bmatrix} \cdot A = \begin{bmatrix} 0 \\ 1 \end{bmatrix} \quad \text{and} \qquad \begin{bmatrix} 0 \\ 1 \end{bmatrix} \cdot A = \begin{bmatrix} 1 \\ 0 \end{bmatrix} \tag{28}$$

We can now calculate the representation array for the whole system including the LC cell. This will be given by the equation:

$$S = N_1 Q_1 M Q_2 N_2 \tag{29}$$

Combining equations (25) and (26) it follows then that:

$$S = \begin{bmatrix} 0 & e^{jk_o d(n+n_o)} \\ e^{jk_o d(n_o+n)} & 0 \end{bmatrix} \tag{30}$$

Using equation (30) we can now calculate the effect of the system on an incoming wave of random polarisation. According to what we said in the beginning of this paragraph, unpolarized light, could be represented by the matrix:

$$IN = \begin{bmatrix} 1 \\ e^{jr(t)} \end{bmatrix} \tag{31}$$

In (31) r(t) is an unknown function of time. The outgoing field then will be given by the equation:

$$\mathrm{OUT} = \mathrm{S} \cdot \mathrm{IN} = \begin{bmatrix} e^{j[k_0 d(n+n_o)+r(t)]} \\ e^{j[k_0 d(n+n_o)+r(t)]} \end{bmatrix} \tag{32}$$

Hence, both components of the output light have the same phase (in agreement with equation (16) and (17)) and therefore polarisation insensitive phase modulation is feasible.

We can easily extend the above idea for a large array of modulating elements. A plane wavefront of unpolarized light, which normally impinges on to such an array of pixels, each of which is characterised by a specific value of tilt angle (by the application of different voltages across it), can be spatially phase modulated. Therefore unpolarised light could give the same refraction pattern that we would normally take using polarised light, and in that sense a two-dimensional, free space, polarisation insensitive, holographic switch using NLC-SLMs is feasible.

The thickness of the liquid crystal pixels has to be chosen such that a continuous shift from phase = 0 to phase = π is possible. Since the tilt angle θ takes values in the interval [0 $\pi/2$], the modulation phase will be:

$$k_0 d(n_o + n_o) + r(t) \le \text{phase} \le k_0 d(n_e + n_o) + r(t)$$

or

$$0 \le \text{phase} \le k_0 d(n_e - n_o) \tag{33}$$

For a π-phase shift we need:

$$k_0 d(n_e - n_o) = \pi$$

or

$$d = \frac{\lambda_0}{2\Delta n} \tag{34}$$

In equation (33), λ_0 is the wavelength of operation in the free space and Δn the birefringence of the nematic liquid crystal. An estimation of the thickness needed for a π-shift can be done for a "standard" nematic liquid crystal such as the E7. Using Wu's formula we can calculate the birefringence of E7 for the telecommunications wavelength window (1,55 μm):

$$\Delta n = 0.196 \tag{35}$$

This will give for the thickness of the cell:

$$d = 3.95\mu m \tag{36}$$

The next step is to see the specific device configurations that will allow for the principle of figure 12 to be implemented. It would be of great advantage in terms of compactness and robustness to incorporate all the elements into a single arrangement. A first possible solution can be seen in figure 13.

The quarter wave plate can be deposited on the pixel array by spin-coating a proper reactive monomer, which can be polymerised by exposure to ultraviolet light. In the cell of figure 13, the Al pad acts as a mirror and also provides the necessary voltage drop across the cell for the liquid crystal to switch.

A second approach is shown in figure 14. The pixel array is integrated on a silicon-1.5μm-transparent backplane device. The quarter wave-plate is positioned in between the front Al mirror and the ITO electrode. Its thickness can be easily adjusted by spin-coating techniques so that it functions as a half-wave plate at λ=1.55 μm.. In applications where the holographic switch is used as a reconfigurable routing device for telecommunication links the wavelength window of operation is quite narrowed

around 1.55 μm, so not significant losses are introduced to the system due to wavelength dispersion and no need for an achromatic wave-plate exists.

Spatial light modulators, such the ones depicted in figure 14, have been already designed and fabricated within our research group. The pixels have been constructed using the polysilicon layer of a conventional 2μm CMOS process. The driving circuitry allows for four different voltage levels and therefore a four-level phase modulation is feasible. Figure 15 shows an overview of the silicon backplane layout.

Finally, in order to increase the liquid crystal response, a twisted nematic LC mixture in a π-cell configuration could be used instead. In such cell the director of the nematic liquid crystal twists along the thickness of the cell through an angle equal to π. In this way flow of material within the cell during the switching process is minimised and the response increases. Given that the thickness of the cell is large enough so that the field can be actually wave-guided through it, the same principle of figure 11 applies and the cell can give fast, polarisation insensitive switching.

In an additional embodiment, a holographic optical switch is formed using reflective hologram devices such as FLC- or NLC-on-semiconductor SLMs, as shown in figure 16. Note that beam-splitters are often used in optical systems to accommodate components such as reflective SLMs. However such beam-splitting components either require the optical signal passing through them to be carefully polarisation controlled, or otherwise introduce 3dB optical loss per pass. Such constraints are typically unacceptable in many optical switching applications. Figure 16 therefore demonstrates a system without the use of beam-splitters.

In figure 16, the usual arrays of inputs (1) and outputs (11) are arranged at the ends of the switch optics. The input signal beams are collimated by a lens (2) as before, and focused back into the output ports by a lens (10) as before. The two hologram devices (5)&(8) are arranged about an interconnect region comprising two lenses (4)&(7) as before, and an additional relay or field lens (6) is added as required. Due to the reflective nature of the hologram devices however, the optical signal beams must now pass twice through lenses (4) and (7) in opposite directions. The inward and outward passes through these lenses must also be spatially or angularly separated, and the optical system therefore takes the basic form of a squashed or upright 'Z' respectively. In addition, lenses (3) and (9) have been added to the switch in order to compensate for these double passes. The combination of lenses (2) and (3) form an optical magnification stage (eg. an objective lens) which projects an image of the input array in front of lens (4). Lens (4) then collimates the beams onto the first SLM (5) and feeds the signals into the interconnect region. Likewise, lens (7) collimates the beams onto the second SLM (8) and feeds the signals to the demagnification stage formed by the combination of lenses (9) and (10).

An ideal CGH is typically a spatial pattern of continuous phase and/or intensity modulation generated by some fixed or reconfigurable display device. In practice, processing limitations in producing CGH patterns, and device limitations in displaying reconfigurable CGH patterns, mean that practical CGHs are typically spatially sampled (eg. pixellated) and then quantised to a discrete number of modulation levels. The most common types of CGH provide phase-only modulation, and are often limited to binary phase capability (eg. $0,\pi$). Because of the non-linear nature of the phase quantisation process, direct calculation of the optimum CGH pattern required to generate a particular pattern of replay is usually impossible, and therefore heuristic iteration techniques such as simulated annealing or error diffusion have often been employed for hologram design.

Iterative CGH design procedures provide a good balance between optimising the replay field generated by a CGH against some target field, whilst broadly minimising the unwanted noise in the replay. However, the inherent randomness that is typically programmed into these algorithms also means that each calculation cycle may create a CGH with unique noise characteristics, ie. the user must intervene at some stage to select the most appropriate hologram for his or her application. This 'hit and miss' approach is not well suited to the use of CGHs for optical switches, where the background noise in the replay field must typically be well quantified in order to prevent crosstalk buildup within the system. This patent is therefore concerned with a design procedure for CGH pattern sets that is suitable for holographic optical switches.

Viewing the diffraction replay image created by a CGH typically involves illuminating the CGH device with coherent or partially-coherent light, and then forming the Fraunhofer far-field diffraction image at some subsequent plane. The most convenient arrangement for achieving this is to illuminate the CGH with collimated perpendicular light, and then to form the replay image in the focal plane of an infinite conjugate-ratio lens as shown in figure 17. According to scalar diffraction theory, the replay image is related to the complex optical transmittance of the CGH device by a scaled 2-dimensional Fourier transform. If the CGH is removed from the system then the lens focuses the light into a single 'zero-order' spot at the centre of the replay field. With the CGH in place, light is diffracted out of this spot into an optical replay distribution of intensity and phase arranged in an (x,y) transverse plane about this zero-order location. In some circumstances, the replay lens may not be present. In these cases, the replay image can be thought of as an angular spectrum of superimposed plane waves.

In a holographic optical switch, the typical requirement for the CGH pattern is for it to produce a replay field with as much optical power concentrated into a single output spot as possible. This condition minimises the routing loss through the switch and is usually achieved by defining a target field for the CGH iteration procedure which contains a single peak at the required replay peak location:

$$\mathrm{Target}(x,y) = \delta(x - X_p, y - Y_p) \tag{37}$$

where δ is the idealised delta-function replay peak profile,
(X_p, Y_p) is the main replay spot location relative to the zero-order position.

In addition, the locations and intensities of all noise peaks within the CGH replay field must also be well quantified in order that the switch can be designed in such a way that this noise does not reach any of the switch output ports – this noise could give rise to crosstalk within the switch. This design problem for holographic switches can be tackled by examining the replay fields for all the CGH patterns that will be required to operate the switch in all configurations. The switch inputs and outputs must then placed in appropriate positions to avoid crosstalk problems. However since the set of required holograms is actually determined by the positions of the inputs and outputs in the first place, this crosstalk minimisation problem is an iterative process by necessity. The complexity of traditional CGH design procedures combined with the complexity of the switch design procedure means that it has not been possible to design large holographic switches according to the prior art knowledge.

In summary, using an iterative CGH design algorithm has several significant drawbacks when applied to optical switching: 1) it is difficult to control the noise distributions in the replay fields that are generated; 2) the CGH design algorithms are numerically intensive to calculate; 3) the target output spot position defined by equation (1) has limited resolution. The last point arises because the target field for the CGH algorithm is typically sampled at the same resolution as (or an integer fraction of) the actual CGH display device. Thus if the hologram display contains M pixels, then the target field also contains a maximum of M discrete and evenly spaced sample points. Using traditional approaches to CGH design, the target peak may only be located on these grid points.

This section describes a non-heuristic method for generating phase-only hologram patterns suitable for optical switch applications, based on the generation and quantisation of a mathematical phase mask. The method allows better resolution for the positioning of the target spot in the replay field, and allows CGHs to be determined rapidly, thereby allowing much greater iteration in the design and placement of the switch input & output ports. In addition, the noise fields generated by CGH patterns designed using this method can be accurately quantified in terms of noise intensity and location.

Phase-only CGHs suitable for optical switches are defined by a pixellated base-cell pattern. This base-cell is directly calculated from the coordinates of the main replay spot for the desired hologram, and is constructed using a rapid phase-quantisation procedure. In order to form the final CGH, the base-cell pattern is tiled or replicated in the (x,y) plane of the hologram display device until the entire aperture of the device is filled. Therefore contrary to other CGH design procedures, the design of the hologram pattern does not directly relate to the resolution of the hologram display device. Instead, the base-cell is typically tiled a non-integer number of times, and generally a different number of times in the x and y directions respectively. As a consequence of this approach, the principal CGH replay mode location is not restricted to a discrete number of locations, but can be placed anywhere within the addresssable region of the CGH replay plane in a quasi-continuous manner.

Furthermore, the design of the base-cell pattern is optimised to maximise the power in a single peak (henceforth called the 'principal mode') of the CGH replay field. The precise location of this peak relative to the zero-order location is used to uniquely define the base-cell design of the hologram according to a deterministic algorithm. Furthermore, the noise properties of the replay field generated by the CGH can typically be described analytically in terms of a summation of regularly spaced peaks (henceforth called modes). Given the direct correspondence between base-cell pattern, principal mode location and noise field, it is then a relatively simple matter to construct procedures to design CGH sets for holographic switches. The speed of CGH generation, and the predictable harmonic structure of the replay field makes this invention highly relevant to the design of holographic switches.

The hologram base cell pattern is calculated from the normalised angular deviation that the CGH is required to impart upon a collimated paraxial beam of light incident upon the hologram pattern. Thus if θ_y & θ_x are the (small-angle) optical diffraction angles of rotation that the CGH is to introduce about the y and x axes respectively then two dimensionless parameters (η_p,ζ_p) that describe the principal replay mode coordinate for the desired hologram can be defined by:

$$\theta_y \approx \frac{\lambda}{P_x}\eta_p \qquad \theta_x \approx \frac{\lambda}{P_y}\zeta_p \tag{38}$$

where λ is the wavelength of light incident upon the CGH,
P is the pixel pitch of the CGH display device (along x & y axial directions).

Alternatively (η_p,ζ_p) may be defined in terms of the physical coordinate of the principal replay spot relative to the zero-order location:

$$X_p = \frac{f\lambda}{P_x}\eta_p \qquad Y_p = \frac{f\lambda}{P_y}\zeta_p \tag{39}$$

where (X_p,Y_p) is the target principal mode location for the hologram,
f is the focal length of the lens used to form the far-field diffraction image.

In order to calculate the base-cell pattern that will route light to according to equations (38) & (39), the normalised target coordinate (η_p,ζ_p) for the principal mode should be written as rational numbers:

$$\eta_p = {}^{N_x}\!/_{D_x} \qquad \zeta_p = {}^{N_y}\!/_{D_y} \tag{40}$$

where N_x, N_y, D_x and D_y are integers.

However according to normal CGH diffraction theory, there is an upper limit on the maximum useful diffraction angle that may be generated by a pixellated hologram pattern. In terms of the normalised target coordinates (η_p,ζ_p), the principal replay mode can only be located within a square region bounded by the corners (–0.5,–0.5) to (+0.5,+0.5) inclusively, where (0,0) represents the zero-order location. The 4 integers that describe the hologram base-cell must therefore satisfy:

$$-\tfrac{1}{2}D_x \le N_x \le \tfrac{1}{2}D_x \qquad -\tfrac{1}{2}D_x \le N_y \le \tfrac{1}{2}D_y \qquad 1 \le D_x \le R_x \qquad 1 \le D_y \le R_y \tag{41}$$

where (R_x,R_y) is the resolution (in number of pixels) of the hologram display device.

For cases where the normalised target coordinate of the principal mode cannot precisely be written as rational fractions, then coordinate (η_p,ζ_p) should be rounded until it does satisfy equations (40) & (41). However it can immediately be seen that there is considerable advantage associated with this invention compared to prior art methods of hologram generation. For example, if $R_x=R_y=25$ pixels, then simulated annealing provides a grid of only 625 locations where the target principal mode can be located. In contrast, the invention provides a potential capability of 10,000 target locations. When $R_x=R_y=100$ then the advantage is even more convincing – 10,000 locations vs. 2,316,484.

D_x and D_y specify the size (number of pixels) of the base-cell pattern required to define the hologram. In general, the smaller the values of D_x and D_y, the more robust the hologram will be against any image errors within the hologram device, and the cleaner the replay field generated, ie. fewer noise peaks will be present in the replay. The rational fractions of equation (40) must be simplified to their lowest denominator forms, or the procedure for generating the base-cell pattern will produce incorrect results, ie. D_x must not be an integer multiple of N_x and D_y must not be an integer multiple of N_y.

The unique base-cell pattern for routing light to coordinate (η_p,ζ_p) is now calculated in 2 steps. Firstly, a spatially-sampled phase-screen ϕ is defined in terms of the above rational fractions. This phase-screen contains $(D_x \times D_y)$ sample points which correspond to the pixels of the base-cell pattern. A typical phase-screen is shown graphically in figure 18.

$$\phi(k,l) = k\frac{N_x}{D_x} + l\frac{N_y}{D_y} \tag{42}$$

where $k = 0,1,2 \ldots (D_x - 1)$, and $l = 0,1,2 \ldots (D_y - 1)$.

In the second step, the phase-screen is phase-quantised to the same number of discrete, uniformly distributed phase-levels, ψ, that are supported by the device that the hologram will be displayed on:

$$\varphi_s(k,l) = \exp(2\pi j \times int\{\phi(k,l) \times \psi\}/\psi) \tag{43}$$

where $\varphi_s(k,l)$ is the final sampled and quantised representation of the base-cell pattern for the target hologram device,
& j is the complex operator $(-1)^{1/2}$,
& $exp(\ldots)$ is the exponential operator,
& $int\{\ldots\}$ is a quantisation function that rounds its argument to the nearest integer towards minus infinity.

Table 2 below gives some design examples of base-cell hologram images for binary-phase and quad-phase devices. Here the base-cell patterns are expressed in terms of the relative phase-angle that the hologram display device must impart at each pixel. These phase angles are defined as:

$$arg\{\varphi_s(k,l)\} = arctan\left\{ Imag\{\varphi_s\} \big/ Real\{\varphi_s\} \right\} \tag{44}$$

	CGH Base-Cell Design, $arg\{\varphi_s(k,l)\}$									
	η_p=0.5, ζ_p=0.5		η_p=0.375, ζ_p= – 0.25 ie. (3/8,-1/4)							
Binary-phase $(\psi = 2)$			0	π	0	0	π	0	π	π
	π	0	π	π	0	π	0	0	π	0
	0	π	π	0	π	π	0	π	0	0
			0	0	π	0	π	π	0	π
Quad-phase $(\psi = 4)$			π/2	π	0	π/2	3π/2	0	π	3π/2
	π	0	π	3π/2	π/2	π	0	π/2	3π/2	0
	0	π	3π/2	0	π	3π/2	π/2	π	0	π/2
			0	π/2	3π/2	0	π	3π/2	π/2	π

Table 2 - Examples of base-cell hologram designs.

Note that the binary-phase representation of the $\eta_p=\zeta_p=0.5$ hologram provides optimum diffraction efficiency, and there is no change in the base-cell pattern for devices with quad-phase modulation capability. In contrast, the CGH design procedure takes full advantage of the better quad-phase device in the second example where $\eta_p=0.375$ and $\zeta_p=-025$.

To form the final hologram image on the display device, the base-cell pattern must be tiled to fill the entire available hologram aperture. This replication will typically occur a non-integer number of times, and generally a different number of times in the x and y directions, figure 19.

Fourier theory predicts that a non-integer number of replications of the base-cell will typically cause a phenomenon known as 'spectral leakage,' whereby a distortion of the spectral domain (ie. the replay field) occurs unless a 'windowing' function is employed. According to this invention, the holograms generated must therefore not be illuminated by plane waves, but must be illuminated by beams

exhibiting apodisation. This apodisation provides the required windowing function and ensures that the replays of the base-cell and of the final hologram image correspond.

One example of a suitable apodisation function is the TEM_{00} Gaussian mode profile. This is the fundamental optical profile emitted by most lasers, waveguides and cleaved fibres. A circularly symmetric TEM_{00} Gaussian intensity profile is usually defined in terms of a beam radius, w, as follows:

$$E_i(x,y) = \left| \exp\left\{ -\frac{x^2+y^2}{w^2} \right\} \right|^2 \tag{45}$$

If this Gaussian field is incident upon a hologram device having a total optical aperture of A, then a useful measure of the effect of the windowing function can be gauged from the parameter γ, where:

$$\gamma = \frac{w}{A} \tag{46}$$

Empirically, it is found that values of $\gamma \approx 3$ and above provide adequate Gaussian apodisation. This Gaussian apodisation meets the windowing function requirement that the optical field intensity must tend towards zero at the edges of the hologram device aperture. Other optical profiles may also be employed provided this condition is met.

Provided the apodisation function is appropriate, then the location of the principal mode generated by the composite tiled hologram will be the same as the location of the principal mode that was used to design the base-cell pattern, subject to any limitations of scalar diffraction theory. In the case of Gaussian apodisation, it is empirically found that approximately 2 complete replications of the base-cell pattern should be present in the final hologram image in order to produce a reliable replay image. However provided this constraint is observed, then the replay spots have profiles determined by the apodisation function, but the spot locations generated by the apodised CGH are the same as predicted by analysis of the base-cell pattern alone.

Holograms designed according to the steps outlined above typically exhibit a regularly spaced array of noise peaks in their replay images. In terms of normalised coordinates, if the principal mode is located at a position denoted by the fraction N/D, then noise modes may also arise at fractional locations n/D, where n is any integer between minus infinity and plus infinity such that $n \neq N$. However not all indicated fractional locations may actually exhibit noise. The presence or absence of a particular noise mode in the hologram replay can be predicted by examining the Fourier series for the base-cell pattern, ie. the presence or absence of specific harmonics in the Fourier series reveals the presence or absence of the corresponding noise modes in the final hologram replay.

Binary-phase holograms are particularly important because they may be displayed on reconfigurable hologram display devices such as ferroelectric liquid-crystal spatial-light-modulators (FLC-SLMs), see ref. [12] for example. The basic modal structure for a binary-phase hologram replay image can be derived analytically from the target peak position coordinates (η_p, ζ_p) using Fourier theory. If D is calculated as the lowest common multiple of D_x and D_y given in equation (40), then the positions and relative intensities of the replay modes are given by:

If D is an even integer:

$$Modes(\eta,\zeta) = Env(\eta,\zeta) \times \sum_{m=1}^{D/2} \sum_{p=-\infty}^{\infty} \sum_{q=-\infty}^{\infty} \left\{ \frac{2}{D\sin\left(\frac{(2m+1)}{D}\pi\right)} \right\}^2 \times \delta\left(p+\eta-(2m+1)\eta_p, q+\zeta-(2m+1)\zeta_p\right)$$

If D is an odd integer:

$$Modes(\eta,\zeta) = Env(\eta,\zeta) \times \sum_{m=1}^{D} \sum_{p=-\infty}^{\infty} \sum_{q=-\infty}^{\infty} \left\{ \frac{0.5}{D\sin\left(\frac{(2m+1)}{2D}\pi\right)} \right\}^2 \times \delta\left(p+\eta-(2m+1)\eta_p, q+\zeta-(2m+1)\zeta_p\right)$$

(47

The function $Env(\eta,\zeta)$ is an intensity envelope function calculated as the optical diffraction image of a single CGH pixel aperture. For square or rectangular pixels, this function is given by:

$$Env(\eta,\zeta)=\left(\tau_x\tau_y\,\mathrm{sinc}(\pi\tau_x\eta)\mathrm{sinc}(\pi\tau_y\zeta)\right)^2 \tag{48}$$

where τ is a pixel "fill-factor" term defined as the ratio of the pixel aperture that modulates light divided by the pixel separation.

Equation (47) only includes the mode locations and signal/noise powers. It does not include the mode-shaping or broadening effects caused by apodisation of the CGH illumination. Analysis of these effects generally requires a full diffraction calculation of the composite hologram image. However, the relatively simple modal representation of the hologram replay distribution derived from the base-cell pattern (and equivalent expressions derived for hologram displays capable of more than 2 phase-levels) is usually adequate to describe the performance of the CGH, and considerably reduces the calculation time required to design hologram sets for optical switches.

In a first embodiment, a reconfigurable CGH pattern designed according to the above procedure is used as an adaptive optical element in order to route an optical beam or signal into an output port, optical receiver or detector. In this case the system comprises the illuminated CGH display, a Fourier replay lens and an output port or ports which are located in the plane of the hologram replay image. A hologram or set of holograms are then displayed in order to locate the principal mode (or other replay mode) into the output port, or in order to maintain routing of light into the output port in the presence of system alignment errors or mechanical perturbations such as vibrations or thermally induced strains. According to the invention, the principal mode can be located into the output port with much greater resolution and precision than is achievable using alternative hologram design techniques. Using this invention, the principal mode can typically be located around the (x,y) plane of the replay image with sub-micron accuracy. This high resolution is particularly important for alignment critical systems such as applications where the output receiver is a single-mode optical fibre.

In a second embodiment, an array of optical receivers or detectors is placed in the replay plane of the hologram and the principal mode (or other replay mode) is scanned about (x,y) in order to characterise the individual positions of the array elements. In this embodiment, a device such as a single-mode fibre array can be tested by varying the CGH in order to maximise the optical return signal in each fibre output and thereby determine the relative positions of the array elements. In this way, it is possible to assess any alignment errors or defects in the locations of the array elements.

In a third embodiment, the principal replay mode (or other replay mode) is scanned about (x,y) in other to determine the numerical aperture, linear aperture, or acceptance mode-distribution of an output receiver or detector.

In a forth embodiment, simulated annealing or other CGH design procedure is applied *to the base-cell pattern* of the hologram (rather than to the hologram itself) in order to suppress a particular noise mode or modes, or otherwise to alter the distribution of optical power within the replay image.

In a fifth embodiment, the shift-invariant nature of the CGH image is utilised in order to change or update the hologram image without altering the replay intensity distribution. In this case, the base-cell pattern is placed at different locations within the CGH aperture before it is tiled to fill the available display aperture. Each CGH thus generated is a shifted and apertured version of the other CGHs, but the replay intensity image remains unaltered to all intensive purposes no matter which hologram is displayed. A further set of hologram patterns can also be calculated such that when they are displayed in sequence, all pixels of the hologram device spend an equal (or otherwise specified) amount of time in each hologram phase state. The sequence may then be repeated for as long as necessary. This embodiment is particularly important for CGH devices such as FLC-SLMs, where the phase-modulating pixels must be continuously switched in order to maintain a net AC voltage at each pixel, but where it may be desirable to maintain a constant replay image.

A simple hologram update scheme is to scroll the hologram pattern (in either 1- or 2-dimensions as appropriate) across the display device by one or more pixels at a time and at regular intervals. The sequence of frames typically repeats when the shifted base-cell pattern used to generate each frame exactly coincides with a tiled version of the base-cell used to generate the first frame, ie. the hologram has shifted by an integer number of base-cell lengths. Figure 20(a) demonstrates a frame sequence for a binary-phase hologram device with 7 pixels displaying a (0.25,0) hologram. In this figure, the base-cell pattern shifts rightwards by 1 pixel between each frame and the next. Note that each column of the sequence in this example achieves an equal overall amount time in each phase state.

For devices such as FLC-SLMs, it may also be desirable to minimise the number of pixels that must undergo phase-state changes per frame change whilst still achieving a near-constant replay field. This is particularly important in applications where there is continuous optical data stream passing through the system. For these applications it may be necessary to "evolve" each frame into the next by altering one, or a group, of pixels at a time, rather than instantaneously displaying the whole of the next frame. Figure 20(b) shows a partial sequence of the extra frames that could be inserted into the sequence of 20(a) in order to reduce the number of pixels that change at a time. In this example, only 1 pixel changes at a time in order to evolve frame #1 of 20(a) into frame #2. Using the sequence of figure 20(b), there may be some distortion of the replay image due to the imperfect intermediate holograms that are introduced. However, such distortion may be minimised by careful choice of the frame sequence.

For some base-cell patterns, simply shifting the hologram may not be sufficient to produce an equal duration in all phase states. In this case, it may be necessary to introduce versions of the base-cell that have been adjusted by a phase-offset of $(2\pi\, u)/\psi$, where u is an integer in the range $1 \ldots \psi$. Because the offset is applied to all pixels, it doesn't alter the replay image. However, it does alter the representation of the base-cell. Figure 20(c) shows an example for a binary-phase (0.2,0) hologram that combines the phase-offset method with frame shifting.

In a sixth embodiment, holograms designed according to the invention or according to any of the embodiments above are used to construct an optical switch. Optical switches are emerging as an important enabling technology for optical networks. Holographic optical switches that use reconfigurable CGHs to route beams of light in free-space between arrays of optical inputs and arrays of optical outputs have several important performance advantages compared to competing technologies such as scalability and high signal to noise margins. A 1xM holographic switch is described in "Polarisation insensitive operation of ferroelectric liquid crystal devices", S.T. Warr and R.J. Mears, Electronics Letters 31:9(1995) p.714-715 and an MxM switch has also been described.

Up until the present time, the complexity of hologram design algorithms, the limited 'resolution' available in the CGH replay field, and the full scalar-wave diffraction theory required to analyse the replay images has made it impossible to design holographic switches with large numbers of inputs and outputs. However, the current invention provides much better prospects for designing these large holographic switches.

According to "Polarisation insensitive operation of ferroelectric liquid crystal devices", S.T. Warr and R.J. Mears, Electronics Letters 31:9(1995) p.714-715, a 1xM switch comprises an input signal which is collimated to illuminate a reconfigurable CGH; a Fourier lens to form the replay image; and an array of optical outputs. The array of outputs are placed in the replay plane of the hologram and various CGH images are displayed in order to route the input signal to one or more of the output ports. The 1xM switch therefore requires a set of at least M different hologram images so that the input signal may be routed to each of the output ports. The switch must be designed in such a way that the outputs coincide with the locations of the principal replay modes of the hologram set, but also in such a way that the noise modes generated by any hologram in this set never gives rise to a significant output signal. The challenge then is to design a set of "orthogonal" holograms suitable for providing the switching function without introducing crosstalk.

Thus, the design of a set of holograms to implement a 1xM switch is reduced to the problem of determining a set of M fractions defined by equation (40) which represent both the CGH patterns required to operate the switch, as well as the proper locations for the output ports as given by equation (39). Typically there are a number of constraints which must be satisfied by the chosen set of fractions, including but not limited to:

- there may be some limit to the minimum allowable physical distance between any pair of output ports related to the physical dimensions (or other property) of these ports,

- there may be some finite number of CGH pixels available which places a limit on the set of fractions that can be considered during the design procedure according to equation (41),

- there may be some maximum allowable variation of optical insertion loss through the switch as it is configured between the various outputs. Because the optical power diffracted into the principal replay mode generally declines with increased angular deflection, this constraint may determine the largest fraction that can be considered in the design,

- there may be some time-limit allocated to complete the design, and therefore less useful fractions such as those with large denominators (which exhibit a greater number of noise modes) may be automatically excluded from the design process,

- there may be additional constraints introduced by the CGH display device, such as the automatic production of a large zero-order spot, which may influence the final choice of fractions,

- there may be some crosstalk specification for the switch which determines how close any noise mode generated by any hologram in the set may be located relative to one of the output ports.

The set of fractions determines both the positions of the output ports and the positions of the noise modes relative to these outputs. In order to minimise crosstalk, the design procedure must therefore be iterative. Thus the search for a suitable set of fractions for the 1xM switch given the above constraints can be solved using a goal-search procedure such as any one of a number of well-known heuristic algorithms (examples include recursive functions and tree-searches). In this case, a simple analytical expression for the location and intensity of the noise modes such as given by equation (47) for binary-phase devices, can greatly reduce the calculation time required to design the hologram set.

A similar approach can also be employed to design MxM switches. An MxM switch comprises an array of optical input signals; an array of reconfigurable CGHs displayed on a first hologram device; a free-space interconnect region; an array of reconfigurable CGHs displayed on a second hologram device; and an array of optical outputs. The input signals are collimated to illuminate the array of CGHs on the first device, are deflected by the hologram images on this device and then propagate across the interconnect region where they are allowed to spatially reorder. The second array of CGHs then deflects the signals into the output ports. In order to route any input to any output, the optical signal must be deflected through some angle at the first CGH device, and then typically through an equal and opposite angle at the second CGH device.

For design of an MxM switch, the input port locations may be represented in normalised coordinates by (η_i,ζ_i) and the output port locations by (η_o,ζ_o). The holograms required to route an input to an output according to the invention are therefore $(\eta_o-\eta_i\,,\,\zeta_o-,\zeta_i)$ and $(\eta_i-\eta_o\,,\,\zeta_i-,\zeta_o)$ displayed in the correct array positions upon the first and second hologram devices respectively. In addition, the first hologram generates a set of noise modes which propagate in different directions and arrive at the second device in various spatial locations. The second hologram also has a set of noise modes which allow different optical propagation directions to reach the output port. Thus for each of the M^2 different connection paths between an input port and an output port, the noise modes generated by the 2 hologram devices must be checked that they do not give rise to an unacceptable crosstalk signal in any of the other output ports.

Thus even using a simplified expression for the noise modes such as equation (47), the iterative placement of input and output ports for an MxM switch is a formidable task. However in many applications it is desirable for the input and output ports to be arranged on a regular grid, eg. $\eta_i=\eta_o={}^1/_{13}$, ${}^2/_{13}$, ${}^3/_{13}$ etc. Unfortunately, the noise modes generated by the holograms required to interconnect ports arranged in a regular fashion tend to route noise straight into other output ports, thereby leading to severe crosstalk problems. The solution disclosed here is to choose a denominator for the fractional locations of the input and output ports which is divisible by 2,3,4, etc. such that the noise mode distribution is more favourable. An example of a 32x32 switch configuration which exhibits very high signal-to-noise margins by using a dnominator of 60 (=3x4x5) is given below.

Input Port Locations (η_i, ζ_i)	**Output Port Locations** (η_o, ζ_o)
$(-{}^{1}/_{60}, -{}^{1}/_{12})$	$(+{}^{1}/_{60}, -{}^{1}/_{12})$
$(-{}^{1}/_{30}, -{}^{1}/_{12})$	$(+{}^{1}/_{30}, -{}^{1}/_{12})$
$(-{}^{1}/_{20}, -{}^{1}/_{12})$	$(+{}^{1}/_{20}, -{}^{1}/_{12})$
$(-{}^{1}/_{60}, -{}^{1}/_{15})$	$(+{}^{1}/_{60}, -{}^{1}/_{15})$
$(-{}^{1}/_{30}, -{}^{1}/_{15})$	$(+{}^{1}/_{30}, -{}^{1}/_{15})$
$(-{}^{1}/_{20}, -{}^{1}/_{15})$	$(+{}^{1}/_{20}, -{}^{1}/_{15})$
$(-{}^{1}/_{60}, -{}^{1}/_{20})$	$(+{}^{1}/_{60}, -{}^{1}/_{20})$
$(-{}^{1}/_{30}, -{}^{1}/_{20})$	$(+{}^{1}/_{30}, -{}^{1}/_{20})$
$(-{}^{1}/_{20}, -{}^{1}/_{20})$	$(+{}^{1}/_{20}, -{}^{1}/_{20})$
$(-{}^{1}/_{60}, -{}^{1}/_{30})$	$(+{}^{1}/_{60}, -{}^{1}/_{30})$
$(-{}^{1}/_{30}, -{}^{1}/_{30})$	$(+{}^{1}/_{30}, -{}^{1}/_{30})$
$(-{}^{1}/_{20}, -{}^{1}/_{30})$	$(+{}^{1}/_{20}, -{}^{1}/_{30})$
$(-{}^{1}/_{60}, -{}^{1}/_{60})$	$(+{}^{1}/_{60}, -{}^{1}/_{60})$
$(-{}^{1}/_{30}, -{}^{1}/_{60})$	$(+{}^{1}/_{30}, -{}^{1}/_{60})$
$(-{}^{1}/_{20}, -{}^{1}/_{60})$	$(+{}^{1}/_{20}, -{}^{1}/_{60})$
$(-{}^{1}/_{60}, 0)$	$(+{}^{1}/_{60}, 0)$
$(-{}^{1}/_{30}, 0)$	$(+{}^{1}/_{30}, 0)$
$(-{}^{1}/_{20}, 0)$	$(+{}^{1}/_{20}, 0)$
$(-{}^{1}/_{60}, +{}^{1}/_{60})$	$(+{}^{1}/_{60}, +{}^{1}/_{60})$
$(-{}^{1}/_{30}, +{}^{1}/_{60})$	$(+{}^{1}/_{30}, +{}^{1}/_{60})$
$(-{}^{1}/_{20}, +{}^{1}/_{60})$	$(+{}^{1}/_{20}, +{}^{1}/_{60})$
$(-{}^{1}/_{60}, +{}^{1}/_{30})$	$(+{}^{1}/_{60}, +{}^{1}/_{30})$
$(-{}^{1}/_{30}, +{}^{1}/_{30})$	$(+{}^{1}/_{30}, +{}^{1}/_{30})$
$(-{}^{1}/_{20}, +{}^{1}/_{30})$	$(+{}^{1}/_{20}, +{}^{1}/_{30})$
$(-{}^{1}/_{60}, +{}^{1}/_{20})$	$(+{}^{1}/_{60}, +{}^{1}/_{20})$
$(-{}^{1}/_{30}, +{}^{1}/_{20})$	$(+{}^{1}/_{30}, +{}^{1}/_{20})$
$(-{}^{1}/_{20}, +{}^{1}/_{20})$	$(+{}^{1}/_{20}, +{}^{1}/_{20})$
$(-{}^{1}/_{60}, +{}^{1}/_{15})$	$(+{}^{1}/_{60}, +{}^{1}/_{15})$
$(-{}^{1}/_{30}, +{}^{1}/_{15})$	$(+{}^{1}/_{30}, +{}^{1}/_{15})$
$(-{}^{1}/_{20}, +{}^{1}/_{15})$	$(+{}^{1}/_{20}, +{}^{1}/_{15})$
$(-{}^{1}/_{60}, +{}^{1}/_{12})$	$(+{}^{1}/_{60}, +{}^{1}/_{12})$
$(-{}^{1}/_{30}, +{}^{1}/_{12})$	$(+{}^{1}/_{30}, +{}^{1}/_{12})$

Table 3 – Input and output port locations for a 32×32 switch.

An alternative technique usable in the invention employs a Fourier Series 'picture' of a beam-steering switch.

The physics is a 2-D version of X-ray diffraction from a crystalline lattice of atoms, so the same notation and analysis methods can be used.

The input to the SLM is the far-field from the fibre or input waveguide, call this Fib(x,y).

The SLM is treated as an infinite, periodic, phase-modulation, Ph(x,y, Λ), of period Λ, multiplied by a top-hat function, Top(x,y), representing the finite extent of the SLM.
Hence the electric field just after phase modulation = Fib(x,y) • Ph(x,y, Λ) • Top (x,y)
= (Fib(x,y) • Top(x,y)) • Ph(x,y, Λ)

where the • represents multiplication.

The output from the switch is the FT (Fourier Transform) of the electric field just after phase modulation = FT(Fib(x,y) • Top(x,y)) * FT (Ph(x,y, Λ))
where the * symbol represents convolution.

Now, because the phase modulation Ph(x,y, Λ) is periodic and of infinite extent, the FT is an infinite set of delta functions of separation in ksinθ space of 2π/Λ, centred on the origin

$$FT(Ph(x,y,\Lambda) = \sum_{i=-\infty}^{\infty} \sum_{j=-\infty}^{\infty} p_{ij}\delta\left(\sin\theta_X - \frac{j\lambda}{\Lambda_X}, \sin\theta_Y - \frac{i\lambda}{\Lambda_Y}\right)$$

where λ is the optical wavelength, θ_X is the beam-steering angle from the x-axis, measured in the x-z plane, θ_Y is the beam-steering angle from the y-axis, measured in the y-z plane. In its most general form Λ can be represented as a vector: Λ_X and Λ_Y are the x and y components of the period vector Λ.

Due to the periodicity of the phase modulation we can use Fourier series to calculate the amplitude, p_{ij}, of each of these delta functions: the answer is exact, assuming diffraction in the Fraunhofer limit. For large beam-steering angles the Fresnel obliquity factor ((1+cosθ)/2) should be included, but SLM pixels are not small enough for this to be relevant. This obliquity factor (which arises from the electromagnetic scattering properties of a Hertzian dipole) is the only fundamental reason for a maximum beam-steering efficiency that decreases with beam-steering angle.

Let the optical system be such that a beam-steering angle θ is converted to a transverse position, L tanθ. Assuming sinθ≈tanθ we then have a set of delta functions at output positions (u,v) given by:

$$FT(Ph(x,y,\Lambda) = \sum_{i=-\infty}^{\infty} \sum_{j=-\infty}^{\infty} p_{ij}\delta\left(u - \frac{jL\lambda}{\Lambda_X}, v_Y - \frac{iL\lambda}{\Lambda_Y}\right)$$

The net output is the above, convolved with the FT(Fib(x,y) • Top(x,y)): call this g(u,v), or in words, the output 'spot'. Hence what we get is g(u,v) (the output spot) replicated all over the output plane with an amplitude (and phase) depending on the value of the Fourier coefficients of the periodic phase modulation:

$$output = \sum_{i=-\infty}^{\infty} \sum_{j=-\infty}^{\infty} p_{ij} g\left(u - \frac{jL\lambda}{\Lambda_X}, v_Y - \frac{iL\lambda}{\Lambda_Y}\right)$$

A transverse translation of the phase modulation Ph(x,y, Λ) changes the phase of the Fourier coefficients p_{ij}, and hence the phase of the output spots, but not their amplitude. As long as the separation of the delta functions is greater than the significant extent (in transverse width)

of the output spots, each spot can be considered independent, and hence the coupling efficiency into the output fibre or waveguide is not affected by transverse translation of the phase modulation. This result, therefore, does not depend on apodisation of the 'aperture' due to the Gaussian nature of the beam incident on the hologram, it is chiefly a function of the relative value of the period, Λ, compared to the hologram width.
To design a switch using beam-steering, the general objective is to position a set of output fibres or waveguides so that for each configuration of the SLM, the selected output fibre or waveguide will receive ONE of these replications of g(u,v) (one of the output spots), and to minimise (or keep below a set threshold) the power coupled from any other (unwanted) replication of g(u,v) into any other output fibre or waveguide.

A method has been previously presented (M J Holmes et al "Low crosstalk devices for wavelength routed networks" IEE Colloquium, June 8th, 1995) so that the unwanted output spots will never couple perfectly (i.e. in perfect alignment) into any other waveguide or output fibre. The method in the paper was for a 1:N beam-steering switch with output into a non-regular 2-D array of output fibres or waveguides. The new method in this patent is:-
(i) a special case of the earlier method allowing beam-steering into a <u>regular</u> 2-D array of output fibres or waveguides. It is this regularity of the output fibre spacing that allows the crosstalk suppression method to be further applied to an N:N switch.
(ii) an extension of the earlier method in that it is recognised that even diffraction orders tend to be very weakly generated, particularly when the period of the phase modulation is an even number of pixels. This increases the number of allowable periods.

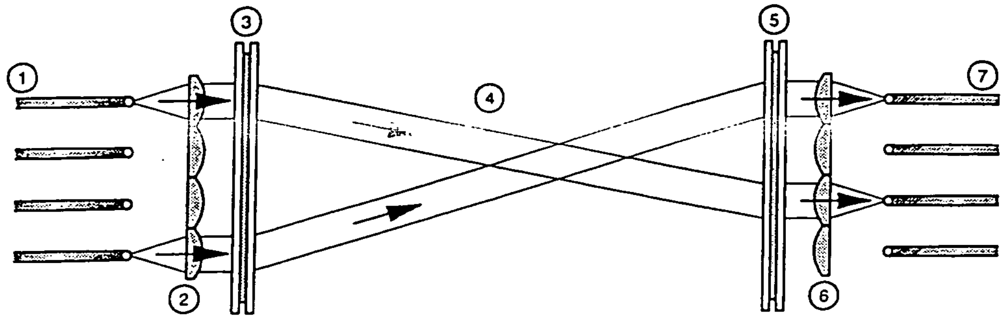

FIGURE 1

1 Array of optical sources
2 Lens array
3 Hologram device
4 Interconnect region
5 Hologram Device
6 Lens array
7 Array of optical sinks

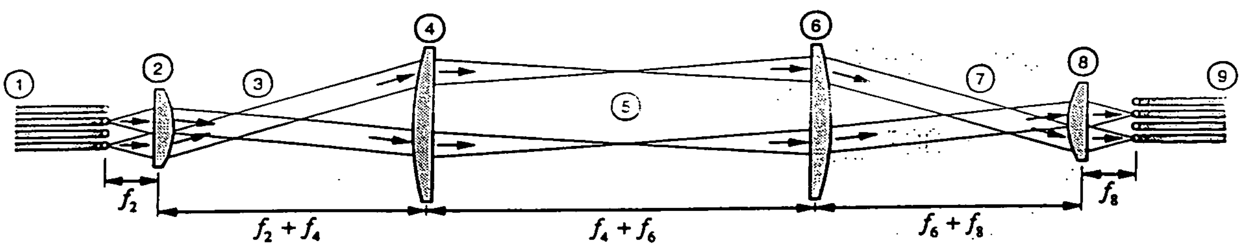

FIGURE 2

1 Array of optical sources
2 Collimating lens
3 Fan-out region
4 Focusing lens
5 Interconnect region
6 Collimating lens
7 Fan-in region
8 Focusing lens
9 Array of optical sinks

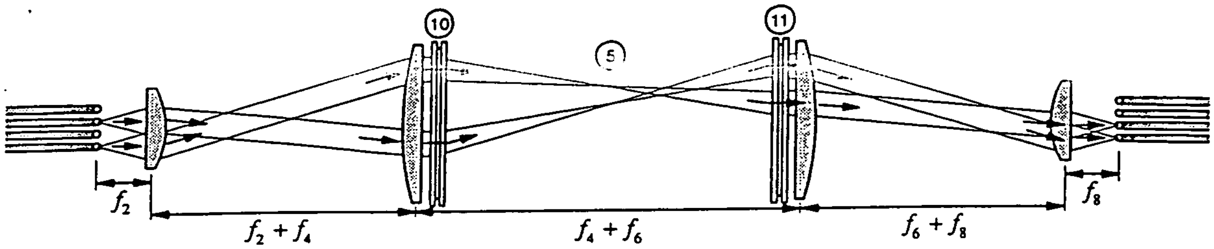

FIGURE 3

5 Interconnect region
10 Hologram device
11 Hologram device

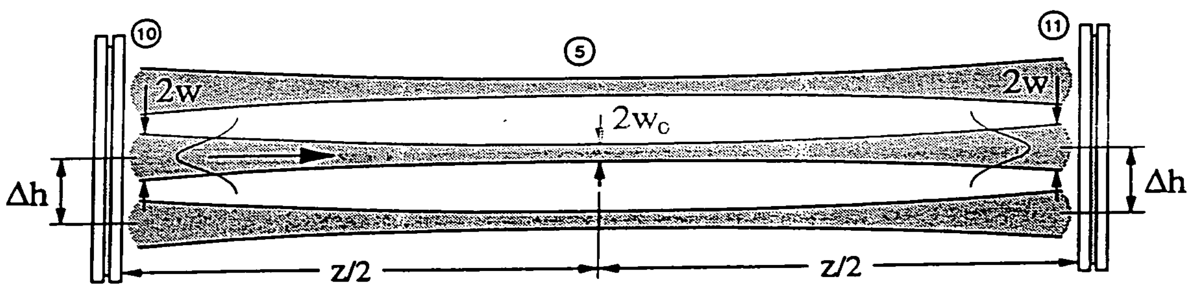

FIGURE 4

5 Interconnect region
10 Hologram device
11 Hologram device

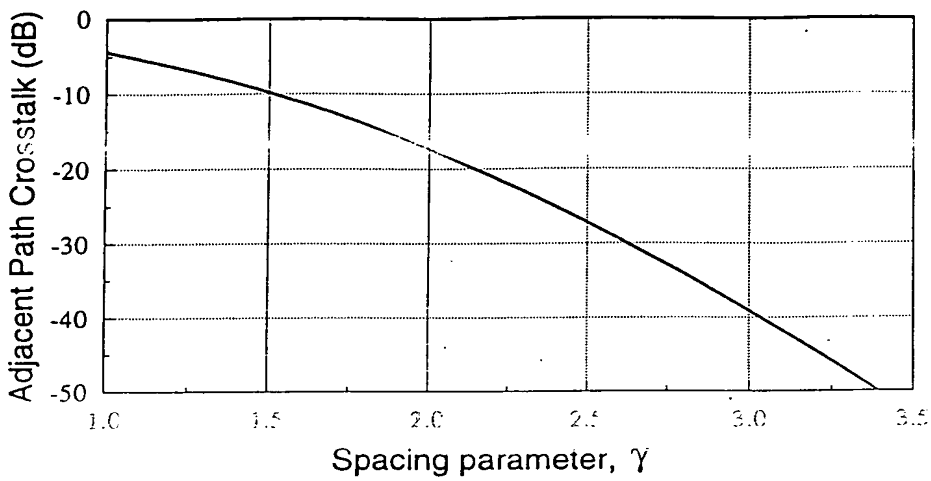

FIGURE 5

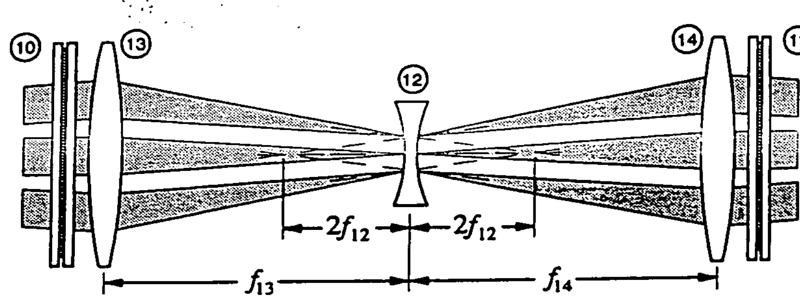

FIGURE 6

(10) Hologram device
(11) Hologram device
(12) Field lens
(13) Focusing lens
(14) Collimating lens

THIS PAGE BLANK (USPTO)

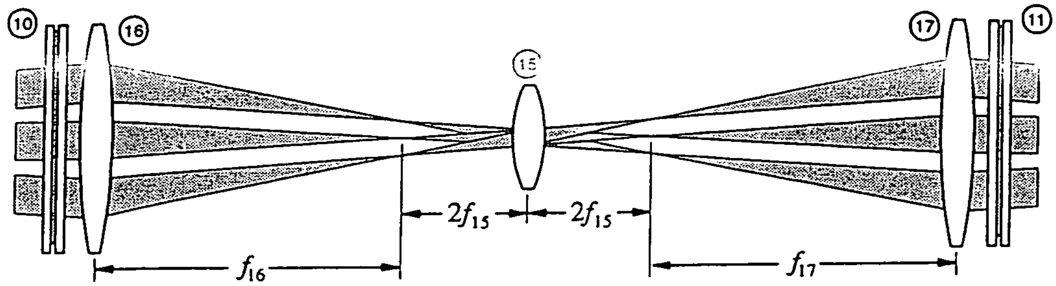

FIGURE 7

(10) Hologram device
(11) Hologram device
(15) Relay lens
(16) Focusing lens
(17) Collimating lens

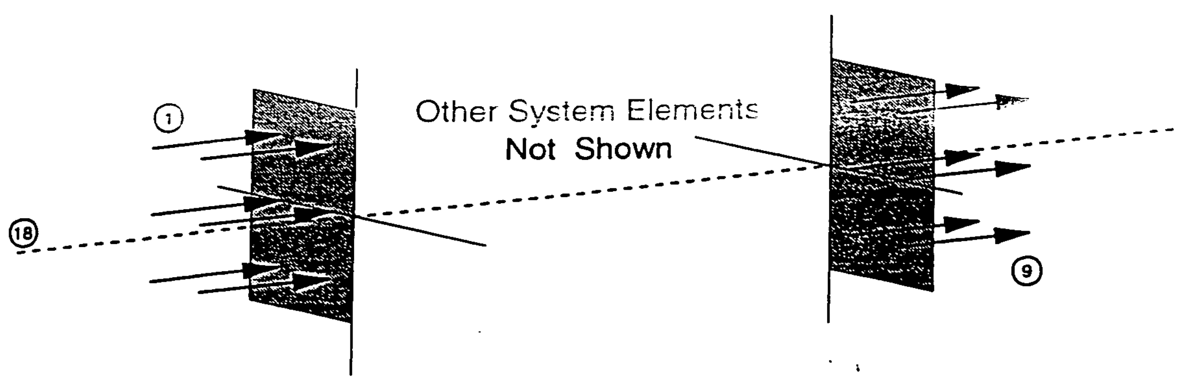

FIGURE 8

(1) Input array
(9) Output array
(18) System optic axis

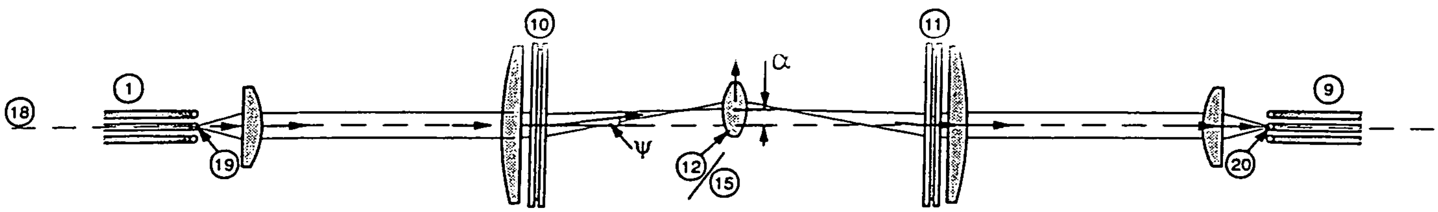

FIGURE 9

1 Array of optical sources
2 Array of optical sinks
10 Hologram device
11 Hologram device
12/15 Field or relay lens
18 Optic axis of system
19 Centre point of input array
20 Centre point of output array

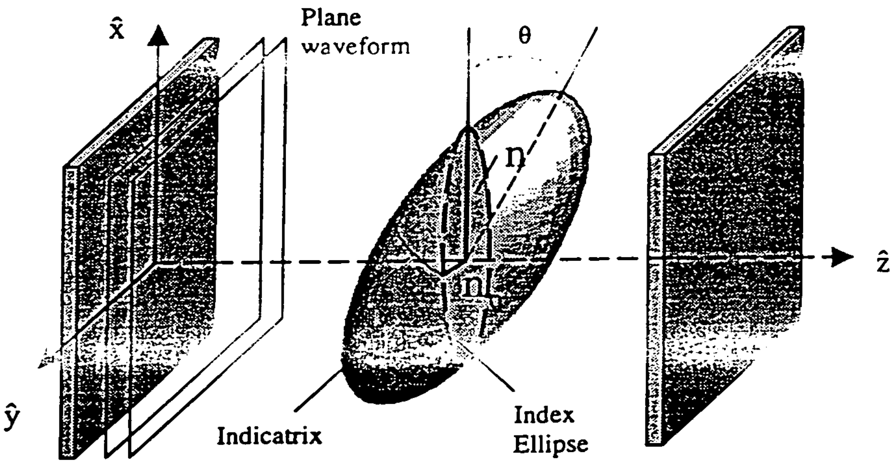

Figure 10 – Propagation of two orthogonal components into a uniaxial medium.

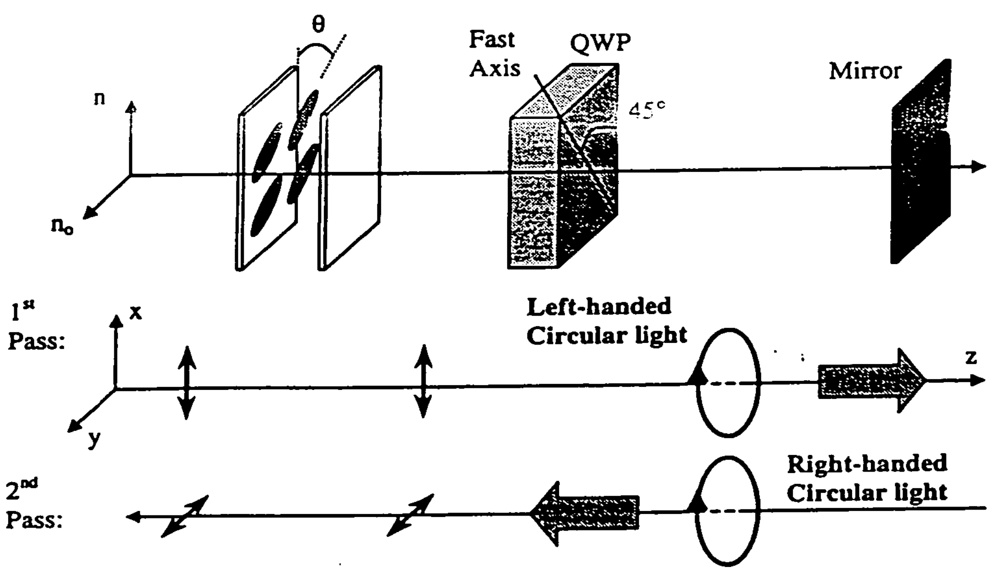

Figure 11 – The polarisation states of the x-component of the input field through the double-pass system

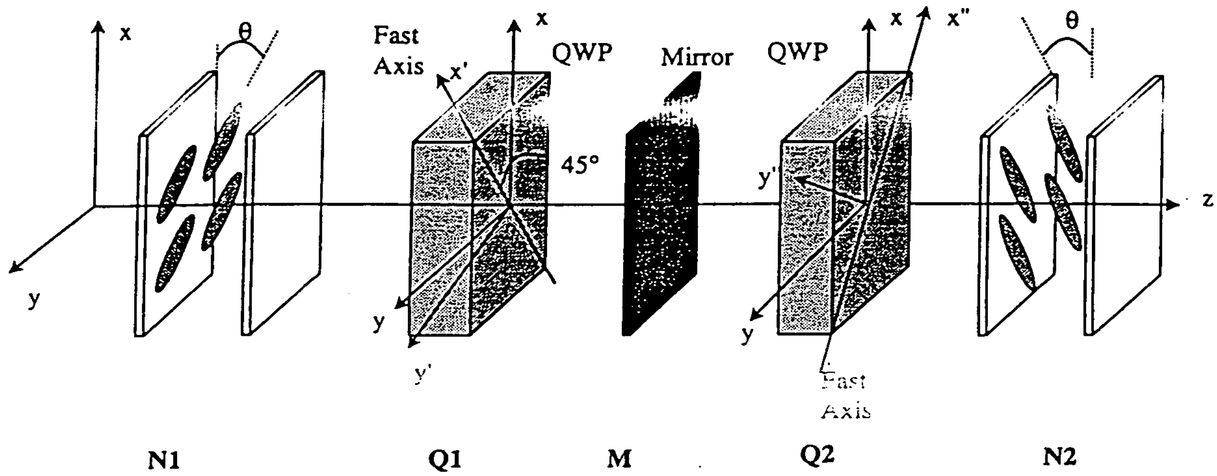

Figure 12- Jones matrix analysis of the system

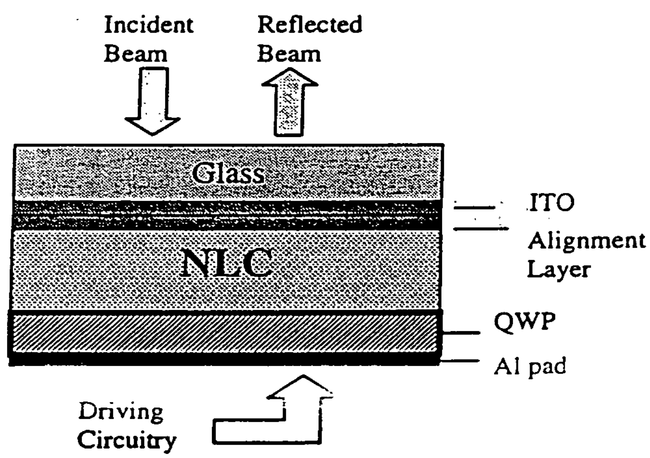

Figure 13 – Element of an active matrix SLM with integrated quarter-wave plate

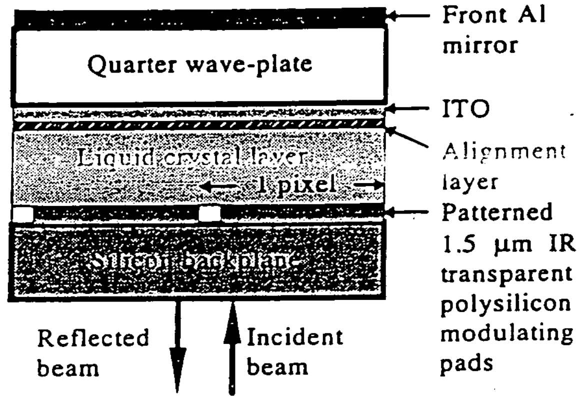

Figure 14 – Integrated double pass SLM on silicon 1.5μm-transparent backplane

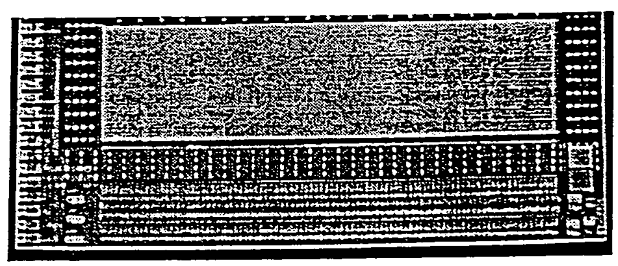

Figure 15 – An overview of the silicon backplane layout

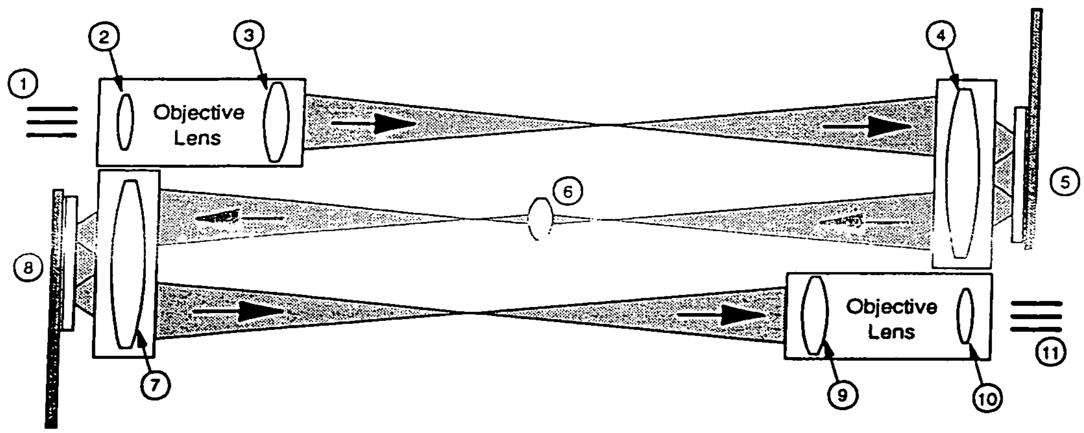

FIGURE 16

1. Array of optical sources
2. Collimating lens
3. Compensation lens
4. Fourier interconnect lens
5. Hologram device
6. Relay or field lens
7. Fourier interconnect lens
8. Hologram device
9. Compensation lens
10. Focusing lens
11. Array of optical sinks

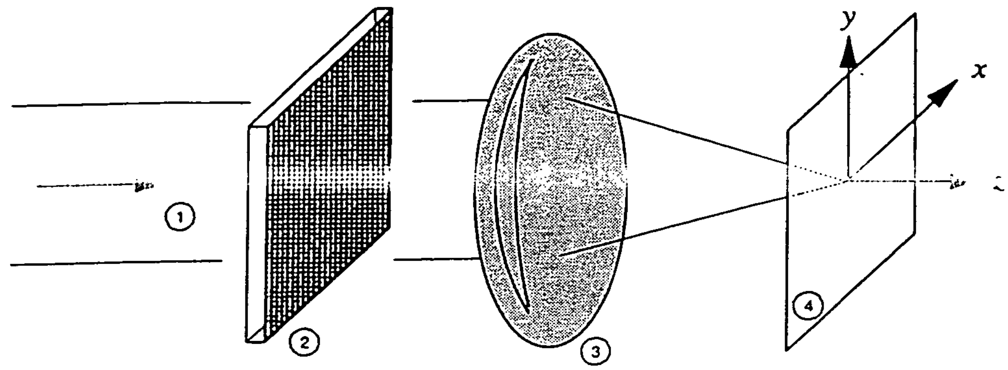

FIGURE 17

1 Collimated light
2 Hologram device
3 Infinite conjugate lens
4 Replay image plane

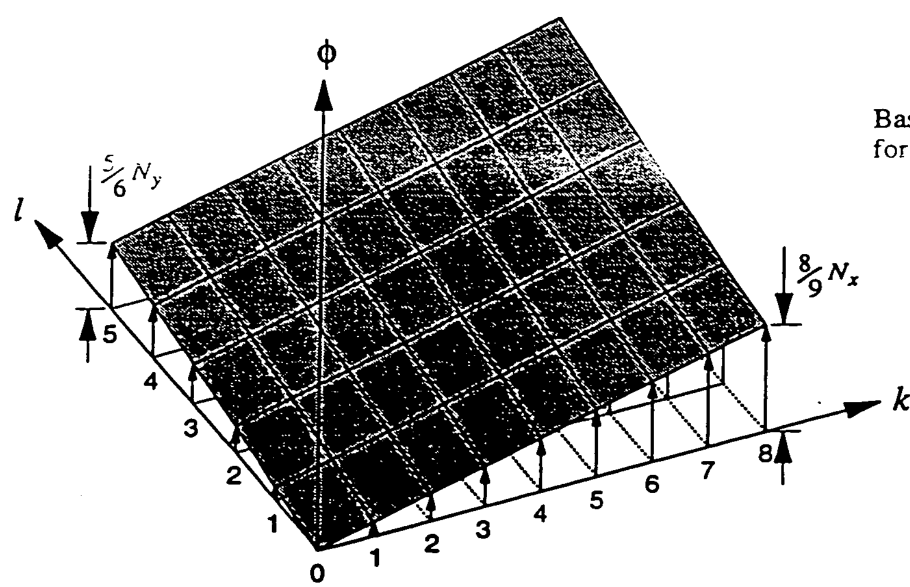

Base-cell phase screen for a hologram where:

$D_x = 9,\ D_y = 6$

FIGURE 18

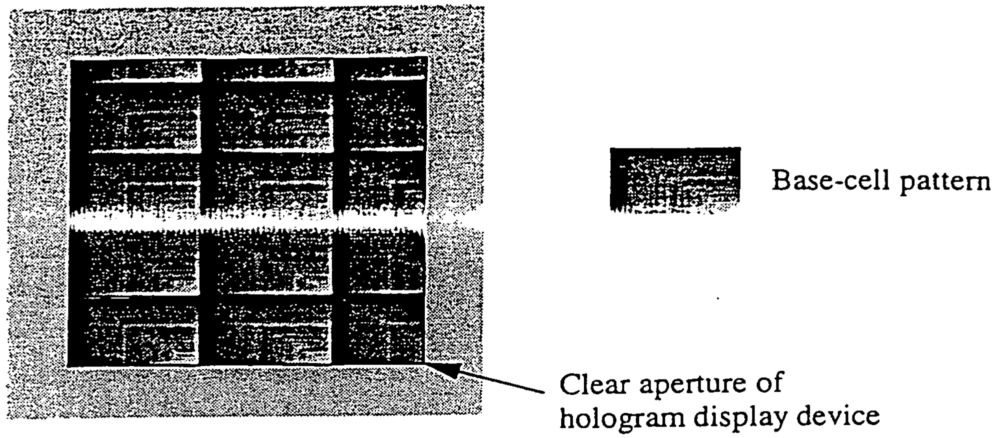

FIGURE 19

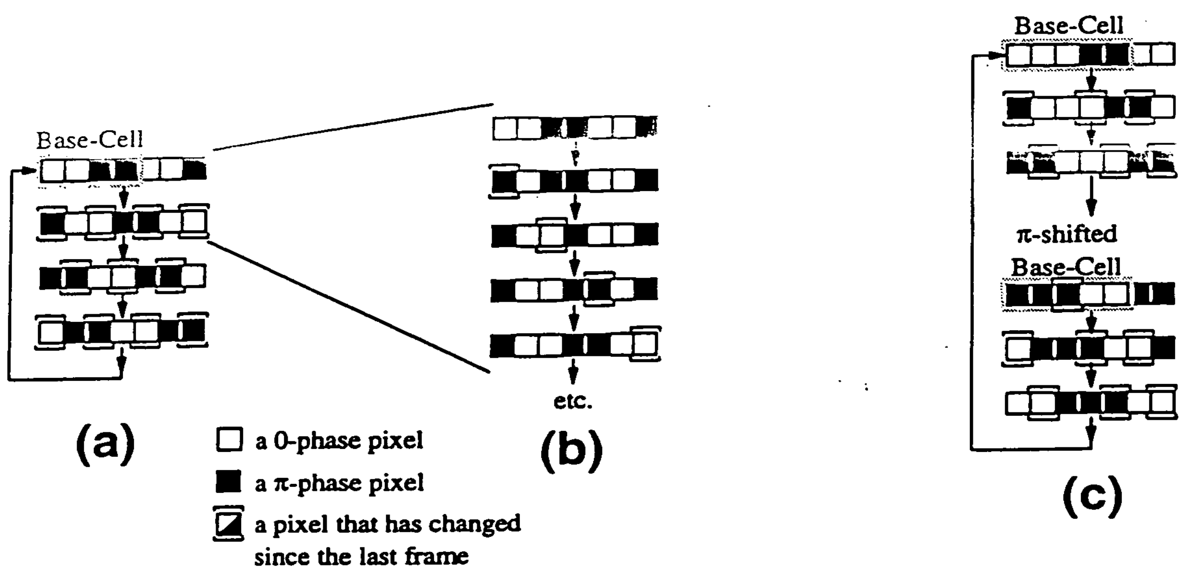

FIGURE 20

PCT/GB00[illegible]3796
Melanie Williams

THIS PAGE BLANK (USPTO)